J. Fluid Mech. (1975), *vol.* 71, *part* 2, *pp.* 209–229
Printed in Great Britain

Finite amplitude axisymmetric thermoconvective flows in a bounded cylindrical layer of fluid

By G. S. CHARLSON AND R. L. SANI
Department of Chemical Engineering, University of Illinois, Urbana

(Received 17 September 1974)

Finite amplitude axisymmetric thermoconvective flows in a bounded cylindrical layer of fluid heated from beneath were calculated using Galerkin's method. Both systems with insulated and with conducting lateral boundaries were investigated for radius-to-depth ratios of 1, 2·25, 2·55 and 2·66. Flows bounded by a conducting lateral boundary were found to be unstable for Rayleigh numbers greater than 1·1 times the critical value. The cell size was found to be an increasing function of the Rayleigh number.

1. Introduction

In earlier papers (Charlson & Sani 1970, 1971) the onset of thermoconvection in a cylindrical fluid layer heated from beneath was studied extensively by means of a linearized stability analysis of the initial quiescent state of the system. Although the linearized stability analysis accurately characterizes the onset of convection, it cannot be presumed to provide an accurate description of finite amplitude motions such as those observed in the laboratory. However, the study of small disturbances leads to predictions of the lowest value of the Rayleigh number at which they will grow exponentially in time, and in the bounded system considered herein, yields the spatial form of the steady small amplitude motion possible in the system when it is very close to the onset of convection.

In reflecting on the physical system, one might pose the following questions. Will the observed flow have a similar form to the motion predicted at the onset, or will that flow itself be unstable to a new disturbance, resulting in a quite different mode for the finite amplitude flow? What changes will the finite amplitude steady-state mode undergo as the temperature gradient across the fluid layer is increased beyond the critical value? How much is the rate of heat transfer enhanced by convection? Is there more than one possible stable flow for a prescribed configuration of the physical system in parameter space? Answers to some of these questions will be sought by a detailed examination of selected axisymmetric flow states of a layer of fluid bounded by a rigid cylindrical enclosure. The interest in axisymmetric finite amplitude flows stems from the work of Koschmieder (1966, 1967, 1969), Liang, Vidal & Acrivos (1969), Hoard, Robertson & Acrivos (1970) and Somerscales & Dougherty (1970), who observed axisymmetric modes in their experiments with cylindrical fluid layers heated from below.

In the supercritical region the amplitude of the motions is not infinitesimal,

linearization of the equations is no longer justifiable and the influence of the nonlinear terms must be accounted for in the analysis. Physically, the primary effect of the nonlinear terms is a modification of the initial exponential growth rate of the disturbances such that in most cases steady motion of finite amplitude is eventually attained. Mathematically, the cellular motions which characterize finite amplitude convection are steady solutions, not uniquely determined by the boundary conditions, to the equations of motion. The indeterminacy is not caused by a lack of constraints, but rather is indicative of a 'branching' of the solution as a function of a parameter of the problem. In the present case the parameter is the Rayleigh number. At Rayleigh numbers below the critical value at the onset of convection, the boundary conditions are sufficient to describe a unique steady solution, i.e. the no-flow solution (Sani 1964; Joseph & Shir 1966). At supercritical values of the Rayleigh number, two or more steady solutions are possible as well as the no-flow solution, which itself remains a possible solution. It has been shown (Sani 1967; Stakgold 1971; Joseph 1971) that the branch, or bifurcation, points of the nonlinear problem can only occur at points corresponding to eigenvalues (Rayleigh numbers) of the linear stability problem. That is, there can exist steady finite amplitude flows at Rayleigh numbers arbitrarily close to the marginal Rayleigh-number stability limits predicted by linear theory. This result has only been rigorously established for those cases in which the eigenvalue is of odd multiplicity and may, or may not, be true in other cases. (Calculations by Charlson & Sani (1970, 1971) suggest that all the eigenvalues, i.e. Rayleigh numbers, predicted by linear theory are simple.) The structure of the finite amplitude flow is close to that of the flow associated with the appropriate solution of the linear stability problem in the sense that the two are identical in the limit of zero flow amplitude (Sani 1967; Joseph 1971).

In order to distinguish the physically realizable solutions among the steady solutions, the stability of the supercritical steady solutions must be investigated.

2. Mathematical characterization

The dimensionless nonlinear equations of motion governing perturbations to the quiescent-state temperature, pressure and velocity field of a fluid in the Boussinesq approximation are

$$Pr^{-1}(\partial/\partial t + \mathscr{R}(\mathbf{u}.\nabla)\,\mathbf{u} = \mathscr{R}T\mathbf{e}_z - \nabla p + \nabla^2\mathbf{u}, \tag{1}$$

$$[\partial/\partial t + \mathscr{R}(\mathbf{u}.\nabla)]\,T = \mathscr{R}(\mathbf{u}.\mathbf{e}_z) + \nabla^2 T, \quad \nabla.\mathbf{u} = 0. \tag{2),(3}$$

Here Pr is the Prandtl number, $\mathscr{R}$ is the square root of the Rayleigh number while the operators ∇ and ∇^2 are defined as in Charlson & Sani (1970) and contain γ, the aspect ratio, i.e. the radius-to-depth ratio of the container. The appropriate boundary conditions, detailed in Charlson & Sani (1970), are those appropriate for either a conducting lateral wall or an insulating lateral wall and in both cases isothermal top and bottom surfaces.

3. Steady solutions

In order to determine the possible steady flow states of (1)–(3), Galerkin's method (Finlayson 1972, p. 10) is used to obtain approximate solutions for prescribed values of the parameters $\mathscr{R}$, Pr and γ. In general, $\mathbf{u}$ and T can be represented by

$$\mathbf{u} = \sum_{i=1}^{K}\sum_{j=1}^{N}\sum_{n=1}^{M} A_{ijn}\mathbf{W}_{ijn} + D_{ijn}\mathbf{V}_{ijn}, \quad T = \sum_{i=1}^{K}\sum_{j=1}^{N}\sum_{n=1}^{M} B_{ijn}\Phi_{ijn}, \quad (4), (5)$$

where

$$\Phi_{ijn}(r,\phi,z) \equiv G_n(\Phi)\, J_n(\alpha_j r)\sin i\pi z, \quad (6)$$

$$\mathbf{W}_{ijn}(r,\phi,z) \equiv G_n(\phi)\,[(\gamma r)^{-1}\, Y_{jn}(r)\, X_i'(z)\,\mathbf{e}_r - (\gamma^{-2}r^{-1})\, Y_{jn}'(r)\, X_i(z)\,\mathbf{e}_z], \quad (7)$$

$$\mathbf{V}_{ijn}(r,\phi,z) \equiv G_n(\phi)\,[-(\gamma r)^{-1} iY_{jn}(r)\, X_i'(z)\,\mathbf{e}_\phi + n(\gamma r)^{-2} Y_{jn}(r)\, X_i(z)\,\mathbf{e}_z]. \quad (8)$$

Here the $Y_{jn}(r)$ are the eigenfunctions of the following eigenvalue problem:

$$\left(\frac{d^2}{dr^2}+\frac{1}{r}\frac{d}{dr}-\frac{(n+1)^2}{r^2}\right)(r^{-1}Y_{jn}(r)) \equiv \xi_{jn}^4 Y_{jn}(r), \quad (9)$$

$$Y_{jn}(r) = Y_{jn}'(t) = 0 \quad \text{for} \quad r = 0, 1. \quad (10)$$

The functions $X_i(z)$ and the α's are defined as in Charlson & Sani (1970) and

$$G_n(\phi) \equiv (2\pi)^{-\frac{1}{2}} \exp[-in\phi]. \quad (11)$$

(Note that the velocity field $\mathbf{u}$ is solenoidal because both $\mathbf{V}_{ijn}$ and $\mathbf{W}_{ijn}$ are solenoidal vector fields.) The problem becomes that of determining the time-independent coefficients A_{ijn}, B_{ijn} and D_{ijn}.

For the specific case of steady *axisymmetric flows* ($n = 0$ states) considered herein, the series representations for the velocity (with $D_{ij0} = 0$) and temperature are substituted into (1) and (2). Premultiplication of the linear momentum equation (1) by $\mathbf{W}_{kl}$ and the energy expression (2) by Φ_{kl} followed by integration over the volume yields the following system of nonlinear algebraic equations to be solved for the $2KN$ coefficients A_{ij} and B_{ij} (the subscript zero has been dropped for convenience):

$$-Pr^{-1}\mathscr{R}\sum_{i,j}\sum_{m,p}\int_V \mathbf{W}_{kl}\cdot(\mathbf{u}_{mp}\cdot\nabla)\,\mathbf{u}_{ij}\,dV + \mathscr{R}\sum_{i,j}\int_V (\mathbf{W}_{kl}\cdot\mathbf{e}_z)\,T_{ij}\,dV$$
$$+\sum_{i,j}\int_V \mathbf{W}_{kl}\cdot\nabla^2\mathbf{u}_{ij}\,dV = 0 \quad (k = 1,\ldots,K;\, l = 1,\ldots,N), \quad (12)$$

$$-\mathscr{R}\sum_{i,j}\sum_{m,p}\int_V \Phi_{kl}(\mathbf{u}_{mp}\cdot\nabla)\,T\,dV + \mathscr{R}\sum_{i,j}\int_V \Phi_{kl}(\mathbf{u}_{ij}\cdot\mathbf{e}_z)\,dV$$
$$+\sum_{i,j}\int_V \Phi_{kl}\nabla^2 T_{ij}\,dV = 0 \quad (k = 1,\ldots,K;\, l = 1,\ldots,N), \quad (13)$$

where $i = 1,\ldots,K$; $j = 1,\ldots,N$; $m = 1,\ldots,K$; $p = 1,\ldots,N$; and

$$\mathbf{u} = \sum_{i,j}\mathbf{u}_{ij} \equiv \sum_{i=1}^{K}\sum_{j=1}^{N} A_{ij}\mathbf{W}_{ij}(r,\phi,z), \quad (14)$$

$$T = \sum_{i,j} T_{ij} \equiv \sum_{i=1}^{K}\sum_{j=1}^{N} B_{ij}\Phi_{ij}(r,\phi,z). \quad (15)$$

It is noteworthy that the pressure does not appear because the solenoidal property of the velocity field $\mathbf{W}_{kl}$, coupled with the boundary conditions and Green's theorem, has been used to eliminate the gradient of the pressure field in (12).

As shown by Liang *et al.* (1969) and Joseph (1971), two steady solutions to (1)–(3) exist for thermoconvection in a confined geometry, one corresponding to upflow at the centre of the fluid layer and the second to downflow at the centre of the fluid layer. After Liang *et al.*, direct substitution of an upflow and downflow solution into the appropriate system of differential equations for the axisymmetric flows considered herein leads to

$$\{u_{rd}(r,z), u_{zd}(r,z), T_d(r,z)\} = -\{-u_{ru}(r,1-z), u_{zu}(r,1-z), T_u(r,1-z)\}. \quad (16)$$

Here the subscripts d and u denote, respectively, the solutions with downflow and upflow at the centre. In terms of the trial solutions (14) and (15), relations (16) are equivalent to obtaining the downflow solution from the corresponding upflow solution simply by a change of sign of all the coefficients (A_{ij} and B_{ij}) of terms which are even about $z = \frac{1}{2}$. It is also noteworthy that the nonlinear system (1)–(3) no longer separates into even and odd solutions about $z = \frac{1}{2}$ as did the linearized system (see Charlson & Sani 1970); consequently the streamlines will no longer be symmetric.

In the case of an insulating lateral boundary, it is convenient to modify the representations (14) and (15) owing to the necessity of including the coefficients of the $\alpha_j = 0$ terms in (6) for $n = 0$; these are non-zero in the nonlinear problem and, in fact, the only terms to account for distortions in the mean temperature field due to the finite amplitude flow, an effect which is not included in a *linear* stability analysis. A straightforward procedure as used in the case of a conducting lateral wall leads to an algebraic system which is difficult to solve.

A more convenient formulation can be obtained by redefining the perturbation temperature T to have a zero mean when averaged over any cross-section $z =$ constant. This property is consistent with the definition of T given in (15) with the $\alpha_j = 0$ root omitted. In this case the expression for the dimensionless temperature field equivalent to $\theta = -z + T$, used in the case of a conducting lateral wall, is replaced by

$$\theta = -z + T_{\mathrm{av}}(z) + T(r,\phi,z), \quad (17)$$

where $T_{\mathrm{av}}(z)$ is defined by

$$\bar{\theta} = -\bar{z} + \overline{T_{\mathrm{av}}(z)} + \overline{T(r,\phi,z)} = -z + T_{\mathrm{av}}(z), \quad (18)$$

an overbar denoting an average over the cross-section.

Substitution of the new expansion (17) for the temperature into (1) and (2) (neglecting the time-derivative terms) yields

$$-Pr^{-1}\mathscr{R}(\mathbf{u}.\nabla)\,\mathbf{u} + \mathscr{R}T(r,\phi,z)\,\mathbf{e}_z + \mathscr{R}T_{\mathrm{av}}(z)\,\mathbf{e}_z + \nabla^2\mathbf{u} - \nabla p = 0, \quad (19)$$

$$-\mathscr{R}(\mathbf{u}.\nabla)\,T(r,\phi,z) - \mathscr{R}(\mathbf{u}.\nabla)\,T_{\mathrm{av}}(z) + \mathscr{R}(\mathbf{u}.\mathbf{e}_z) + \nabla^2 T(r,\phi,z) + \nabla^2 T_{\mathrm{av}}(z) = 0. \quad (20)$$

If (19) is averaged over a cross-section, then

$$-\mathscr{R}(u_z\overline{T'_{\mathrm{av}}(z)}) - \mathscr{R}\overline{(\mathbf{u}.\nabla T(r,\phi,z))} + \mathscr{R}\overline{(\mathbf{u}.\mathbf{e}_z)} + \overline{\nabla^2 T(r,\phi,z)} + T''_{\mathrm{av}}(z) = 0, \quad (21)$$

where a prime denotes differentiation with respect to z. Making use of the solenoidal character of the velocity field, the boundary conditions and Green's theorem in a plane leads to

$$T''_{\mathrm{av}}(z) = \mathscr{R}(\overline{\mathbf{u}.\nabla T(r,\phi,z)}). \tag{22}$$

Integrating twice and applying Green's theorem yields

$$T_{\mathrm{av}}(z) = \mathscr{R}\left(\int_0^z (u_z T(r,\phi,z)\,dz - z\langle u_z T(r,\phi,z)\rangle\right), \tag{23}$$

where angular brackets signify an average over the volume. Therefore (20) can be simplified to

$$\nabla^2 T(r,\phi,z) + \mathscr{R}(\mathbf{u}.\mathbf{e}_z) - \mathscr{R}(u_z(u_z T(r,\phi,z)) - u_z\langle u_z T(r,\phi,z)\rangle) - \mathscr{R}(\mathbf{u}.\nabla T(r,\phi,z) + \overline{\mathbf{u}.\nabla T(r,\phi,z)}) = 0. \tag{24}$$

On substitution of (23) and the definition

$$\nabla\hat{p} \equiv \nabla p_{\mathrm{av}} + \nabla p = \mathscr{R}(\mathbf{u}.\nabla T(r,\phi,z)) + \nabla p,$$

the equation (19) for the rate of change of linear momentum becomes

$$-Pr^{-1}\mathscr{R}(\mathbf{u}.\nabla)\,\mathbf{u} + \mathscr{R}T(r,\phi,z)\,\mathbf{e}_z + \nabla^2\mathbf{u} - \nabla\hat{p} = 0. \tag{25}$$

(Note that in general p_{av} is *not* the pressure averaged over the cross-section.) The final versions of the equations, (24) and (25), have the same linear forms and properties as the linearized system of equations solved in Charlson & Sani (1970) since $T_{\mathrm{av}}(z) = 0$ for the linearized system. Thus the mean temperature field is handled 'exactly', that is, for given approximate fluctuating fields the mean temperature field is determined exactly. The resulting mean temperature field is more accurate than a Galerkin approximation which includes the mean field in the expansion representation. For the case of an insulating lateral wall the Galerkin equation (12) remains the same but (13) is replaced by

$$-\mathscr{R}\sum_{i,j}\sum_{m,p}\int_V \Phi_{kl}(\mathbf{u}_{mp}.\nabla)\,T_{ij}\,dV - \int_V \Phi_{kl}(\overline{\mathbf{u}_{mp}.\nabla T_{ij}})\,dV + \mathscr{R}\sum_{q,r}\left(\int_V \Phi_{kl}u_{zmp}(u_{zqr}T_{ij})\,dV - \int_V \Phi_{kl}u_{zmp}\langle u_{zqr}T_{ij}\rangle\,dV\right) + \sum_{i,j}\int_V \Phi_{kl}(\mathbf{u}_{ij}.\mathbf{e}_z)\,dV + \sum_{i,j}\Phi_{kl}\nabla^2 T_{ij}\,dV = 0 \quad (k = 1,\ldots,K;\ l = 1,\ldots,N). \tag{26}$$

In all cases a method detailed by Broyden (1965) was used to solve the resulting system of nonlinear algebraic equations.

4. Characterization of steady solutions: the vitality and the Nusselt number

The finite amplitude convection synthesized from the solution of the system of nonlinear algebraic equations for the coefficients in the representations of the velocity and temperature can be characterized by two parameters. The first,

the vitality A of the physical system, measures the departure of the system from the initial quiescent state. To indicate simply its origin, consider (1) and (2). If (1) is premultiplied by the fluctuating velocity $\mathbf{u}$ and added to (2) premultiplied by the fluctuating temperature T, then

$$Pr^{-1}\mathbf{u}.\frac{\partial \mathbf{u}}{\partial t}+T\frac{\partial T}{\partial t}=\mathscr{R}[2(\mathbf{u}.\mathbf{e}_z)T-\mathbf{u}.(\mathbf{u}.\nabla)\mathbf{u}-T(\mathbf{u}.\nabla)T]+\mathbf{u}.\nabla^2\mathbf{u}+T\nabla^2T. \quad (27)$$

Integrating (27) over the volume and rearranging the left side gives

$$\frac{1}{2}\frac{\partial}{\partial t}\int_V (Pr^{-1}\mathbf{u}.\mathbf{u}+T^2)\,dV=-\int_V [\nabla\mathbf{u}.(\nabla\mathbf{u})^\dagger+\nabla T.\nabla T]\,dV$$
$$-2\mathscr{R}\int_V (\mathbf{u}.\mathbf{e}_z)T\,dV-\mathscr{R}\int_V [\mathbf{u}.(\mathbf{u}.\nabla)\mathbf{u}+T(\mathbf{u}.\nabla)T]\,dV. \quad (28)$$

The right side of this expression contains only terms related to the generation or dissipation of energy. The left side, resembling an expression for the time rate of change of kinetic energy, would vanish in the marginal stability state in which all perturbations are assumed to be infinitesimal in magnitude. Hence a stationary value of

$$A\equiv\int_V (Pr^{-1}\mathbf{u}.\mathbf{u}+T^2)\,dV, \quad (29)$$

called the vitality, characterizes the onset of convection and for finite amplitude flows its magnitude increases with increasing flow amplitude. (It is noteworthy that the parameter $\epsilon\equiv PrA$ appears as a small expansion parameter in the perturbation analysis of convection in vessels of arbitrary shape by Joseph 1971.)

A second characteristic parameter of the finite amplitude convection is the Nusselt number Nu:

$$Nu|_{z_0}\equiv 1-[\partial\overline{T}/\partial z]_{z_0}+\mathscr{R}[\overline{u_zT}]_{z_0}. \quad (30)$$

In the case of an insulating lateral boundary, T in (30) is the total perturbation to the linear temperature profile, i.e. $T=T_{\mathrm{av}}(z)+T(r,\Phi,z)$. The departure of the Nusselt number from unity measures the modification of the heat flux due to the convective process and it is convenient to evaluate the Nusselt number at the top and bottom plates since $\overline{u_zT}$ vanishes there:

$$Nu|_{z=0,1}=1-[\overline{\partial T/\partial z}]_{z=0,1}. \quad (31)$$

For an insulating side wall, $Nu|_{z=0}$ is identically equal to $Nu|_{z=1}$ (no lateral heat losses from the system allowed). However, for a conducting side wall, heat may be lost through the side wall by warmer fluid rising near the wall, or heat may be gained through the side wall if cool fluid falls near the wall.

5. Stability of steady states

A linear stability analysis similar to that used in the investigation of the stability of the initial quiescent state in Charleson & Sani (1970, 1971) is employed to investigate the stability of the steady solutions of the nonlinear system of

governing equations (1)–(3). That is, the steady axisymmetric flow state, defined by the velocity and temperature pair $(\mathbf{u}, T)$, is subjected to a small time-dependent disturbance of the form $(\mathscr{U}(t,r,\phi,z), \mathscr{T}(t,r,\phi,z))$. If, as time increases, the amplitude of this pair decreases to zero, the system is linearly asymptotically stable to that form of disturbance. If, on the other hand, the pair $(\mathscr{U}, \mathscr{T})$ grows in time, the system is unstable.

To implement this analysis, the dimensionless velocity, temperature and pressure fields are defined to be the sum of the steady-state solution and an infinitesimal time-dependent quantity:

$$\mathbf{u}(t,r,\phi,z) = \mathbf{u}(r,\phi,z) + \mathscr{U}(t,r,\phi,z), \quad T(t,r,\phi,z) = T(r,\phi,z) + \mathscr{T}(t,r,\phi,z), \tag{32), (33}$$

$$p(t,r,\phi,z) = p(r,\phi,z) + \mathscr{P}(t,r,\phi,z). \tag{34}$$

These time-dependent fields, when substituted into (1)–(3), lead to

$$Pr^{-1}\partial\mathscr{U}/\partial t + \mathscr{R}(\mathscr{U}.\nabla\mathbf{u} + \mathbf{u}.\nabla\mathscr{U}) = \mathscr{R}\mathscr{T}\mathbf{e}_z - \nabla\mathscr{P} + \nabla^2\mathscr{U}, \tag{35}$$

$$\partial\mathscr{T}/\partial t + \mathscr{R}(\mathscr{U}.\nabla T + \mathbf{u}.\nabla\mathscr{T}) = \mathscr{R}(\mathscr{U}.\mathbf{e}_z) + \nabla^2\mathscr{T}, \tag{36}$$

$$\nabla.\mathscr{U} = 0, \tag{37}$$

where second-order terms in the disturbance parameters $\mathscr{U}, \mathscr{T}$ and $\mathscr{P}$ have been neglected. The disturbance parameters are also constrained to satisfy the appropriate boundary conditions for either an insulating or a conducting lateral boundary. Note that, since $\mathbf{u}$ and T are known quantities, the system of equations (35)–(37) is linear in the unknown perturbations $\mathscr{U}$ and $\mathscr{T}$. For the case of an insulating side wall in which the steady and disturbance temperature fields are partitioned into a horizontal mean field and a field with zero horizontal mean

$$(\mathscr{T} = \mathscr{T}_{\mathrm{av}}(t,z) + \mathscr{T}(t,r,\phi,z)),$$

the equation (36) for the rate of change of energy becomes

$$\partial\mathscr{T}/\partial t + u_z(\mathscr{U}_z T + u_z\mathscr{T}) - u_z\langle u_z\mathscr{T}\rangle - u_z\langle\mathscr{U}_z T\rangle - \overline{\mathscr{U}.\nabla T} - \overline{\mathbf{u}.\nabla\mathscr{T}} + \mathscr{U}.\nabla T + \mathbf{u}.\nabla = \mathscr{R}(\mathscr{U}.\mathbf{e}_z) + \nabla^2\mathscr{T} \tag{38}$$

and the equation of motion is identical to (35).

The equations of the linearized stability analysis and the appropriate boundary conditions are non-separable, and to generate a solution recourse is made to the Galerkin method. The infinitesimal disturbances $(\mathscr{U}, T)$ to the steady-state functions are represented in the form

$$\mathscr{U}(t,r,\phi,z) = \sum_{i,j,n} \mathscr{U}_{ijn}(t,r,\phi,z) \equiv \sum_{i=1}^{I}\sum_{j=1}^{J}\sum_{n=1}^{M} A_{ijn}(t)\,\mathbf{W}_{ijn}(r,\phi,z) + D_{ijn}(t)\,\mathbf{V}_{ijn}(r,\phi,z), \tag{39}$$

$$\mathscr{T}(t,r,\phi,z) = \sum_{i,j,n} \mathscr{T}_{ijn}(t,r,\phi,z) \equiv \sum_{i=1}^{I}\sum_{j=1}^{J}\sum_{n=1}^{M} B_{ijn}(t)\,\Phi_{ijn}(r,\phi,z), \tag{40}$$

where the functions $\mathbf{W}_{ijn}$, $\mathbf{V}_{ijn}$ and Φ_{ijn} have the forms given in (6), (7) and (8), respectively, and hence satisfy all boundary constraints on the velocity and temperature fields.

The values of A_{kl} and B_{kl} corresponding to the steady state to be analysed are known from the nonlinear analysis and the time-dependent coefficients

A_{ijn}, D_{ijn} and B_{ijn} in the perturbation velocity and temperature fields are the solutions of the following system of ordinary differential equations generated via the Galerkin procedure:

$$\sum_{i,j,n}\left[Pr^{-1}\int_V \mathbf{X}_{rsm}\cdot\frac{\partial \mathscr{U}_{ijn}}{\partial t}\,dV + Pr^{-1}\mathscr{R}\sum_{k,l}\left(\int_V \mathbf{X}_{rsm}\cdot(\mathscr{U}_{ijn}\cdot\nabla\mathbf{u}_{kl})\,dV + \int_V \mathbf{X}_{rsm}\cdot(\mathbf{u}_{kl}\cdot\nabla\mathscr{U}_{ijn})\,dV\right) - \mathscr{R}\int_V \mathbf{X}_{rsm}\cdot(\mathscr{T}_{ijn}\mathbf{e}_z)\,dV - \int_V \mathbf{X}_{rsm}\cdot\nabla^2\mathscr{U}_{ijn}\,dV\right] = 0 \quad (r = 1,\ldots,I,\ s = 1,\ldots,J), \quad (41),(42)$$

$$\sum_{i,j,n}\left[\int_V \tilde{\Phi}_{rsm}\frac{\partial \mathscr{T}}{\partial t}\,dV + \mathscr{R}\sum_{k,l}\left(\int_V(\tilde{\Phi}_{rsm}\mathscr{U}_{ijn}\cdot\nabla T_{kl})\,dV + \int_V \tilde{\Phi}_{rsm}(\mathbf{u}_{kl}\cdot\nabla\mathscr{T}_{ijn})\,dV\right) - \mathscr{R}\int_V \tilde{\Phi}_{rsm}(\mathscr{U}_{ijn}\cdot\mathbf{e})\,dV - \int_V \tilde{\Phi}_{rsn}\nabla^2\mathscr{T}_{ijn}\,dV\right] = 0 \quad (r = 1,\ldots,I, s = 1,\ldots,J). \quad (43)$$

Here $\mathbf{X}_{rsm}$ is either $\tilde{W}_{rsm}$ or $\tilde{V}_{rsm}$ and a tilde denotes a complex conjugate.

Since the system of differential equations (35)–(37) is linear and invariant with respect to a translation of the origin in time, an exponential time dependence of the following form is assumed for $A_{ijn}(t)$, $D_{ijn}(t)$ and $B_{ijn}(t)$:

$$A_{ijn}(t) = A_{ijn}e^{\sigma t}, \quad D_{ijn}(t) = D_{ijn}e^{\sigma t}, \quad B_{ijn}(t) = B_{ijn}e^{\sigma t}.$$

Substitution of these representations into (41)–(43) results in an algebraic eigenvalue problem to be solved for the eigenvalues σ. If all the eigenvalues σ have negative real parts, then a disturbance of the form assumed, i.e. a disturbance having an angular dependence of the form $e^{n\phi}$, for n of the selected value, will decay in time and the axisymmetric steady solution is said to be stable to disturbances of that form. If one, or more, of the eigenvalues has a positive real part, then the disturbance will grow exponentially. In this case the steady solution is unstable and therefore not likely to be observed experimentally. It should be emphasized that the stability analysis here is by no means complete since only selected disturbances ($n = 0, 1, 2, 3, 4$) have been investigated.

6. Sample results and discussion

Using (12) and (13) or (26) the velocity and temperature coefficients for selected values of γ, $\mathscr{R}^2$ and Pr were calculated with $K = 4$ and $N = 5$ ($N = 4$ for case of $\gamma = 1{\cdot}0$ with a conducting lateral wall) in (14) and (15), i.e. for five (four for $\gamma = 1{\cdot}0$ with a conducting lateral wall) radial trial functions and four vertical trial functions. This choice of trial solution for $\gamma = 2{\cdot}66$ leads to a critical Rayleigh number of 1805·92 compared with the value 1803·32 obtained in Charlson & Sani (1970) with $K = 10$ and $N = 5$, or an error in the critical Rayleigh number of less than 1 %. The structure of the linearized velocity field is also duplicated with an error of less than 1 % between the two representations. While no error bounds

$\mathscr{R}^2$	Pr	Solution branch	Radial rolls	Direction of flows†	A‡	$Nu\|_0$	$Nu\|_1$	Stability§
2548·7	—	1	1	—	0·0	First linear solution		—
7361·2	—	2	1‖	—	0·0	Second linear solution		—
2600	1·0	1	1	*D*	2·144	1·043	0·976	*S*
3000	1·0	1	1	*D*	6·463	1·192	0·973	*S*
6000	1·0	1	1	*D*	18·899	1·785	1·167	*S*
7500	1·0	1	1	*D*	22·534	1·918	1·256	$S, U(n=2)$
2600	0·2	1	1	*D*	4·042	1·021	0·985	$S, U(n=2)$
2600	0·025	1	1	*D*	4·571	1·003	0·997	*S*
3000	0·025	1	1	*D*	16·768	1·013	0·990	*S*
6000	0·025	1	1	*D*	97·537	1·117	0·958	$S, U(n=2)$
7500	0·025	1	1	*D*	144·409	1·199	0·948	$S, U(n=2)$
2600	10·0	1	1	*D*	0·0387	1·049	0·975	*S*
2600	60·0	1	1	*D*	0·0381	1·050	0·974	*S*
2800	60·0	1	1	*D*	0·0815	1·146	0·969	*S*
3000	60·0	1	1	*D*	0·106	1·224	0·979	*S*
4500	60·0	1	1	*D*	0·185	1·657	1·104	*S*
7410	1·0	2	2¶	*D*	1·901	1·028	0·982	*U*
7510	1·0	2	2¶	*D*	3·328	1·055	0·975	*U*

† *D*, downflow at centre of fluid layer.

‡ For $Pr < 1$, A is $Pr^{\frac{1}{2}}$ times A defined by (29).

§ *S*, stable to infinitesimal disturbances; *U*, unstable (the value of the wavenumber n is included for non-axisymmetric cases).

‖ Two rolls in vertical, one in radial direction.

¶ Transition between number of rolls given and one less.

TABLE 1. Nonlinear results for conducting lateral wall; aspect ratio $\gamma = 1{\cdot}0$

$\mathscr{R}^2$	Pr	Solution branch	Radial rolls	Direction of flow†	A‡	$Nu\|_0$	$Nu\|_1$	Stability§
1810·3	—	1	2	—	0·0	First linear solution		—
2137·1	—	3	3	—	0·0	Second linear solution		—
2864·6	—	3	2	—	0·0	Third linear solution		—
1840	1·0	3	2	*U*	1·462	1·009	1·000	—
1900	1·0	1	2	*U*	2·666	1·025	1·008	—
2200	1·0	1	2	*U*	6·732	1·124	1·064	—
2400	1·0	1	2	*U*	8·946	1·203	1·109	—
2600	1·0	1	2	*U*	10·922	1·285	1·154	—
2900	1·0	1	2	*U*	13·520	1·403	1·220	*S*
1900	0·025	1	2	*U*	7·293	1·001	0·999	—
2000	0·025	1	2	*U*	13·559	1·004	0·998	—
2100	0·025	1	2	*U*	17·590	—	—	*S*
1840	60·0	1	2	*U*	0·0296	1·010	1·001	—
2000	60·0	1	2	*U*	0·0797	1·059	1·027	*S*, *U* ($n = 3, 4$‖)
2150	1·0	2	3	*U*	—	0·997	1·014	*U*
2250	1·0	2	3	*U*	4·486	1·019	1·070	—
2400	1·0	2	3	*U*	6·862	1·060	1·142	—
2880	1·0	3	3¶	*U*	0·596	1·001	1·001	*U*
2900	1·0	3	3¶	*U*	1·261	1·003	1·002	—

† *D*, downflow at centre of fluid layer; *U*, upflow at centre of fluid layer.

‡ For $Pr < 1$, A is $Pr^{\frac{1}{2}}$ times A defined by (29).

§ *S*, stable to infinitesimal disturbances; *U*, unstable (the value of the wavenumber n is included for non-axisymmetric cases).

‖ Fastest growing.

¶ Transition between number of rolls given and one less.

TABLE 2. Nonlinear results for conducting lateral wall; aspect ratio $\gamma = 2{\cdot}55$

$\mathscr{R}^2$	Pr	Solution branch	Radial rolls	Direction of flows †	A‡	$Nu\|_0$	$Nu\|_1$	Stability§
1805·9	—	1	3	—	0·0	First linear solution		—
2088·7	—	2	3	—	0·0	Second linear solution		—
2748·4	—	3	4	—	0·0	Third linear solution		—
1840	1·0	1	3	*U*	1·537	1·009	1·002	—
1880	1·0	1	3	*U*	2·344	1·018	1·008	$S, U(n = 4)$‖
2100	1·0	1	3	*U*	5·473	1·079	1·050	$S, U(n = 3, 4$‖$)$
2200	1·0	1	3	*U*	6·663	1·112	1·073	—
2200	1·0	1	3	*D*	6·663	1·073	1·112	$S, U(n = 3, 4$‖$)$
2300	1·0	1	3	*D*	7·770	1·096	1·147	$S, U(n = 3, 4$‖$)$
2350	1·0	1	3	*D*	8·301	1·107	1·165	*S*
2400	1·0	1	3¶	*U*	8·822	1·184	1·118	*S*
2400	1·0	1	3¶	*D*	8·822	1·118	1·184	$S, U(n = 3, 4$‖$)$
2500	1·0	1	3¶	*U*	9·844	1·224	1·140	—
2550	1·0	1	2	*U*	10·348	1·244	1·150	—
2600	1·0	1	2	*U*	10·844	1·266	1·161	$S, U(n = 4)$
2600	1·0	1	2	*D*	10·844	1·161	1·266	—
2800	1·0	1	3	*U*	12·727	1·351	1·204	*S*
1880	60·0	1	3	*U*	0·047	1·020	1·009	$S, U(n = 3, 4$‖$)$
2000	60·0	1	3	*U*	0·080	1·054	1·032	$S, U(n = 3, 4$‖$)$
2200	60·0	1	3	*U*	0·119	1·121	1·078	$S, U(n = 3, 4$‖$)$
2300	60	1	3¶	*U*	0·136	1·158	1·101	—
2350	60	1	3¶	*U*	0·143	1·177	1·113	*S*
2400	60	1	3¶	*U*	0·150	1·197	1·124	$S, U(n = 3, 4$‖$)$
2450	60	1	3¶	*U*	0·157	1·218	1·136	—
2500	60	1	3¶	*U*	0·164	1·234	1·147	*S*
1840	0·025	1	3	*U*	3·693	1·000	1·000	*S*
1880	0·025	1	3¶	*U*	6·220	1·001	0·999	*S*
1950	0·025	1	3¶	*U*	10·768	1·002	0·999	*S*
2000	0·025	1	2	*U*	13·548	1·003	0·998	$S, U(n = 2)$
2050	0·025	1	2	*U*	15·608	1·004	0·997	—
2075	0·025	1	3¶	*U*	15·608	1·005	0·997	*S*
2088·73	0·025	1	3¶	*U*	75·196	—	—	$U, U(n = 2)$
2100	0·025	1	3¶	*U*	15·205	1·004	0·997	*U*

† *D*, downflow at centre of fluid layer; *U*, upflow at centre of fluid layer.

‡ For $Pr < 1$, A is $Pr^{\frac{1}{2}}$ times A defined by (29).

§ *S*, stable to infinitesimal disturbances; *U*, unstable (the value of the wavenumber n is included for non-axisymmetric cases).

‖ Fastest growing.

¶ Transition between number of rolls given and one less.

TABLE 3. Nonlinear results for conducting lateral wall; aspect ratio $\gamma = 2{\cdot}66$

were obtained for the supercritical flows investigated, comparison with previous linear results (Charlson & Sani 1970) as well as with qualitative features of certain numerical simulations (Gershuni, Zhukovitskii & Tarunin 1966; Tarunin 1967; Liang *et al.* 1969) gives confidence in the results in the neighbourhood of the branch points and guarded confidence further along the supercritical branch. Steady axisymmetric solutions were obtained for aspect ratios of 1·0, 2·55 and 2·66 and Prandtl numbers of 0·025, 1·0 and 60·0 for a conducting boundary.

$\mathscr{R}^2$	Pr	Solution branch	Radial rolls	Direction of flow†	A	$Nu\|_0$	$Nu\|_1$	Stability‡
2090	1·0	1	3	*U*	0·481	0·998	1·003	*U*
2090	1·0	2	3	*D*	0·481	1·003	0·998	*U*
2095	1·0	2	3	*U*	—	0·997	1·009	—
2098	1·0	2	3	*U*	—	0·997	1·011	—
2100	1·0	2	3	*U*	1·447	0·997	1·013	*U*
2105	1·0	2	3	*U*	—	0·997	1·017	—
2110	1·0	2	3	*U*	—	0·997	1·021	—
2125	1·0	2	3	*U*	2·601	1·000	1·031	—
2175	1·0	2	3	*U*	4·021	1·011	1·060	—
2250	1·0	2	3	*U*	5·512	1·032	1·100	—
2500	1·0	2	3	*U*	8·857	1·100	1·219	—
2100	60·0	2	3	*U*	—	0·9947	1·019	*U*
2105	60·0	2	3	*U*	—	0·9966	1·017	—
2750	1·0	3	4	*U*	0·334	1·001	0·999	*U*
2760	1·0	3	4	*U*	0·861	1·004	0·999	—
2800	1·0	3	4	*U*	1·752	1·011	1·001	—

† *D*, downflow at centre of fluid layer; *U*, upflow at centre of fluid layer.
‡ *U*, unstable to axisymmetric disturbances.

TABLE 4. Nonlinear results for conducting lateral wall; aspect ratio $\gamma = 2{\cdot}66$

For the case of an insulating boundary, results were obtained for aspect ratios of 1·0 and 2·25 and Prandtl numbers of 0·025 and 1·0. Certain features of the resulting flows are given in tables 1–4. The stability of selected steady solutions to infinitesimal axisymmetric and non-axisymmetric disturbances of azimuthal wavenumbers $n = 1, 2, 3$ and 4 was investigated.

The streamlines and isotherms corresponding to the finite amplitude solution for a layer of fluid with $Pr = 1$ are displayed in figures 1 and 2 for an aspect ratio of unity and Rayleigh numbers of 2600 and 6000. (The abscissa (ordinate) of all figures displaying streamlines or isotherms covers the range $0 \leqslant r \leqslant 1$ ($0 \leqslant z \leqslant 1$) in equal increments.) The convection manifests itself as a single radial roll completely filling the cylinder. From figure 1 it is evident that the structure of the flow near the critical state (the approximate critical Rayleigh number is 2549) is modified only slightly by increasing the Rayleigh number to 6000. The corresponding modification to the mean temperature field is similar to Goldstein's (1964) observations and indicates that the motion transfers heat in such a manner that the average temperature gradient in the central region of the fluid layer is decreased. The latter decreases the gravitational potential energy available for conversion into kinetic energy of a new flow, which stabilizes the basic flow to other disturbances. Such an effect stabilizes the flow consisting of one radial roll to axisymmetric and selected non-axisymmetric disturbances at all Rayleigh numbers investigated except 6000, at which it becomes unstable to a disturbance of azimuthal wavenumber $n = 2$. The second steady solution, corresponding to points along a branch bifurcating from the second eigenvalue of the linear problem, is possible for Rayleigh numbers greater than 7361.

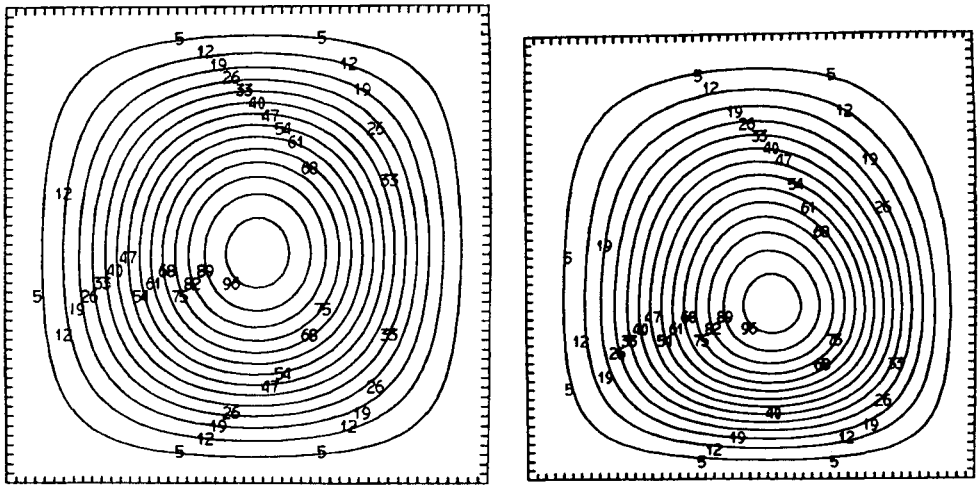

(a) (b)

FIGURE 1. Streamlines for downflow solution with a conducting lateral wall; $\gamma = 1{\cdot}0$, $Pr = 1{\cdot}0$. (a) $\mathscr{R}^2 = 2600$. (b) $\mathscr{R}^2 = 6000$.

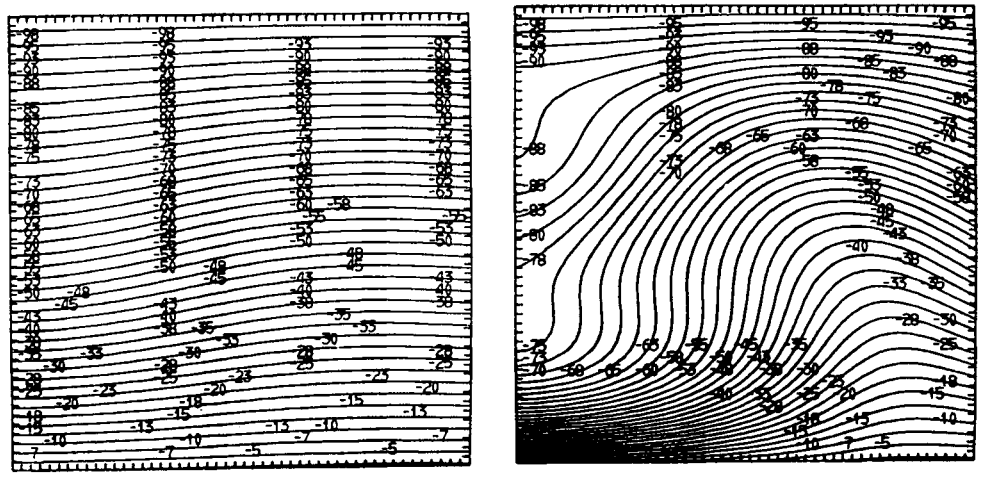

(a) (b)

FIGURE 2. Isotherms for downflow solution with a conducting lateral wall; $\gamma = 1{\cdot}0$; $Pr = 1{\cdot}0$. (a) $\mathscr{R}^2 = 2600$. (b) $\mathscr{R}^2 = 6000$.

However, this second energy state, which corresponds to two radial rolls stacked in the vertical, is not stable even to axisymmetric disturbances.

The Prandtl number has little effect on the flow structure predicted at an aspect ratio of one, but its effect is evident in the characteristic parameters, the vitality and the Nusselt number, which are displayed in figures 3 and 4, respectively, for the first energy state and Prandtl numbers of 0·025, 1·0 and 6·0. At $Pr = 0{\cdot}025$, which is approximately the value for mercury, which has a kinematic

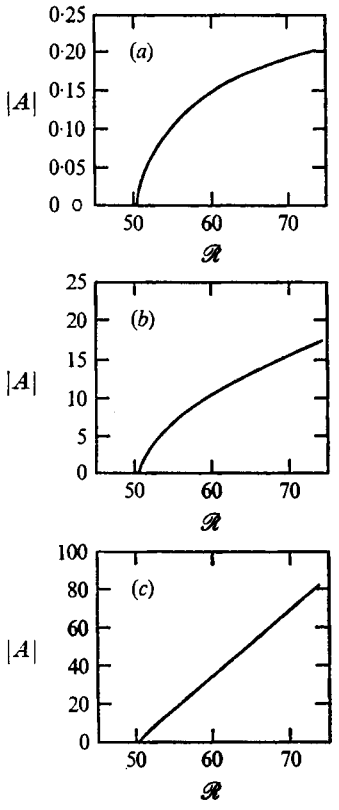

FIGURE 3

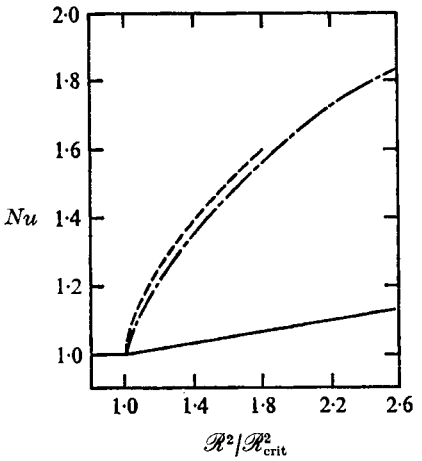

FIGURE 4

FIGURE 3. Branch diagram for a conducting lateral wall; $\gamma = 1{\cdot}0$. (*a*) $Pr = 60$. (*b*) $Pr = 1$. (*c*) $Pr = 0{\cdot}025$.

FIGURE 4. Nusselt number at $z = 0$ for downflow solution with a conducting lateral wall; $\gamma = 1{\cdot}0$. – – –, $Pr = 60$; — · —, $Pr = 1$; ——, $Pr = 0{\cdot}025$.

viscosity about a factor of ten smaller than water but has a thermal conductivity nearly twenty times larger, the vitality is significantly larger than it is for Prandtl numbers of 1 or 60. This effect suggests that the fluid velocities resulting from the small viscous effects are quite pronounced.

The Nusselt number results for $Pr = 0{\cdot}025$, as indicated in figure 4, are significantly less than those for the higher Prandtl numbers. The initial rate of increase in heat flux by convection (the dimensionless heat flux being the product of the Nusselt number and Rayleigh number) is only 1·09 for $Pr = 0{\cdot}025$ compared with 2·28 for $Pr = 1{\cdot}0$ and 2·48 for $Pr = 60$. These results are qualitatively similar to the experimental results of Rossby (1969) for thin fluid layers. He measured initial rates of increase in the heat flux of 1·28 for mercury ($Pr = 0{\cdot}025$), 2·45 for water ($Pr = 6{\cdot}8$) and 2·50 for a silicone oil ($Pr = 200$). Results for various aspect ratios are tabulated in table 5. The low Nusselt number, indicating a small increase in heat transfer due to convection, and the large vitality, suggesting relatively high convective velocities for low Prandtl number fluids, suggest that the

Aspect ratio	Lateral boundary	Flow direction	Pr	Initial slope†
1·00	Conducting	Down	0·025	1·09
1·00	Conducting	Down	1·00	2·28
1·00	Conducting	Down	60·0	2·49
2·55	Conducting	Up	0·025	1·04
2·55	Conducting	Up	1·00	1·53
2·55	Conducting	Up	60·0	1·62
2·66	Conducting	Up	0·025	1·03
2·66	Conducting	Up	1·00	1·46
2·66	Conducting	Up	60·0	1·51
1·00	Insulating	—	1·00	1·26
2·25	Insulating	—	1·00	1·37
2·25	Insulating	—	0·025	1·01
‡	Insulating	—	0·025	1·28
‡	Insulating	—	6·8	2·45
‡	Insulating	—	200	2·50

† In conducting cases, initial slope is evaluated at bottom surface.

‡ Experimental results of Rossby in fluid layers of depths less than 1 cm and diameters of $8\frac{3}{4}$ in.

TABLE 5. Initial rate of increase in heat flux by convection.

thermal conductivity, not viscous effects, is the controlling quantity in determining the effect of convection on the heat transfer in low Prandtl number fluids.

For the case of an insulating lateral wall and an aspect ratio of 2·25, the first three axisymmetric states according to linear theory occur at $\mathscr{R}^2 = 1794{\cdot}9$ (a dynamic state of two radial rolls), $\mathscr{R}^2 = 2325{\cdot}6$ (three radial rolls) and $\mathscr{R}^2 = 2735{\cdot}0$ (one radial roll). The finite amplitude solution at a slightly supercritical Rayleigh number consists of two radial rolls as the second and third energy states are unstable to axisymmetric disturbances in this range of Rayleigh numbers. (These and additional results for an insulated lateral wall are tabulated in tables 6 and 7.) As the Rayleigh number is increased the outer roll increases slightly in size and the velocities within it increase more rapidly, but the gross character of the flow changes only slightly The Nusselt number for the system, reflecting the increase in heat transfer as a result of convection, is predicted to be a convex function of the Rayleigh number and the rate of heat transfer has increased by about 14 % owing to an increase in the Rayleigh number to 1·5 times the critical value. It is not surprising that the increase in the rate of heat transfer due to convection is smaller than that given by Silveston (1963), since his experiments were conducted in thin fluid layers in which the effects of the lateral walls were negligible. At an aspect ratio of 2·25, rigid walls exert a stronger stabilizing influence, which is reflected in the large critical Rayleigh number, and hence convection is not as highly developed. As before, the effect of a Prandtl number of 0·025 is seen primarily in the vitality and Nusselt number.

A most interesting case is that of a cylindrical fluid layer of aspect ratio 2·66 bounded by perfectly conducting walls. A linear stability analysis leads to a critical Rayleigh number of 1805·9 for the order of approximation considered here and to an instability in the form of three radial rolls, the outermost being

$\mathscr{R}^2$	Pr	Solution branch	Radial rolls	A†	Nu	Stability‡
2264·0	—	1	1	0·0	First linear solution	
6656·9	—	2	1§	0·0	Second linear solution	
2300	1·0	1	1	1·913	1·004	*S*
2400	1·0	1	1	3·863	1·015	*S*
2600	1·0	1	1	6·517	1·037	*S*
3000	1·0	1	1	—	1·076	*S*
4000	1·0	1	1	20·245	1·156	*S*
6000	1·0	1	1	37·356	1·261	*S*
7000	1·0	1	1	45·274	1·297	*S*
2300	60	1	1	0·064	1·014	*S*
2300	0·025	1	1	—	1·000	*S*
2500	0·025	1	1	—	1·000	*S*

† For $Pr < 1$, A is $Pr^{\frac{1}{2}}$ times A defined by (29).
‡ *S*, stable to infinitesimal axisymmetric disturbances.
§ Two rolls in vertical, one in radial direction.

TABLE 6. Nonlinear results for insulating lateral wall: aspect ratio $\gamma = 1{\cdot}0$.
(Flow direction not indicated since upflow and downflow solution have same properties.)

$\mathscr{R}^2$	Pr	Solution branch	Radial rolls	A†	Nu	Stability‡
1794·9	—	1	2	0·0	First linear solution	
2325·6	—	2	3	0·0	Second linear solution	
2735·0	—	3	1	0·0	Third linear solution	
1850	1·0	1	2	1·338	1·011	—
2000	1·0	1	2	2·578	1·038	—
2200	1·0	1	2	3·613	1·072	—
2400	1·0	1	2	4·398	1·102	—
2600	1·0	1	2	5·050	1·130	*S*
2800	1·0	1	2	2·944	1·155	*S*
1825	0·025	1	2	—	1·000	—
1850	0·025	1	2	—	1·000	—
1900	0·025	1	2	—	1·000	—
2000	0·025	1	2	—	1·001	*S*
2100	0·025	1	2	—	1·001	—
2200	0·025	1	2	—	1·001	—
2400	0·025	1	2	—	1·002	*S*
2350	1·0	2	3	—	1·004	*U*
2400	1·0	2	3	—	1·013	—
2750	1·0	3	1	—	1·002	*U*

† For $Pr < 1$, A is $Pr^{\frac{1}{2}}$ times A defined by (29).
‡ *S*, stable to infinitesimal axisymmetric disturbances; *U*, unstable.

TABLE 7. Nonlinear results for insulating lateral wall; aspect ratio $\gamma = 2{\cdot}25$.
(Flow direction not indicated since upflow and downflow solution have same properties.)

small. (The second and third axisymmetric states obtained from a linear analysis, $\mathscr{R}^2 = 2088{\cdot}7$ and $2748{\cdot}4$, correspond, respectively, to spatial patterns with three radial rolls with an inner roll slightly smaller than the other two and a transitional pattern which approaches four radial rolls.) The branching curve for $Pr = 1$ for upflow at the centre for this case is displayed in figure 5. The broken lines for

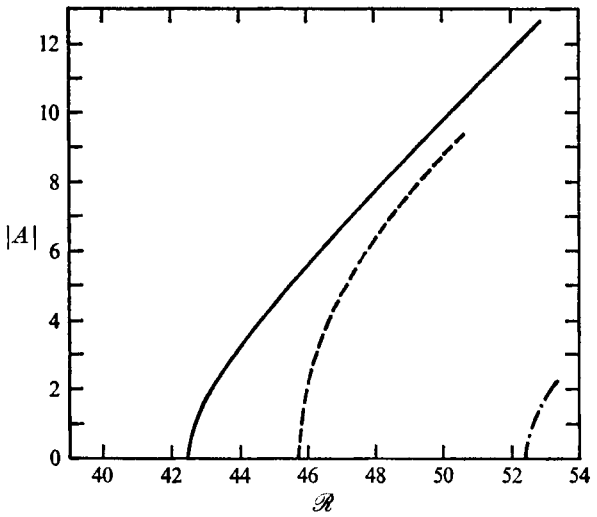

FIGURE 5. Branch diagram for a conducting lateral wall; $\gamma = 2{\cdot}66$, $Pr = 1{\cdot}00$.

the second and third branches indicate that solutions on these branches are unstable. (It should be pointed out that a number of non-axisymmetric solution branches are predicted to occur in the $\mathscr{R}$ range of figure 5 and thus are not displayed, nor was their stability determined.)

The solutions along the first branch are characterized in figures 6–8, where the streamlines and isotherms corresponding to successively larger supercritical Rayleigh numbers for a Prandtl number of 1·0 are displayed. In figure 6, at a Rayleigh number of 1880, the three-roll structure is similar to that of the linear state. As the Rayleigh number increases the inner two rolls grow until at a Rayleigh number of 2400 (figure 7) the outer roll has been pinched off at the centre, forming two small rolls in each corner. (Somewhat similar corner vortices have also been predicted by Tarunin 1967.) The inner rolls continue to grow until at $\mathscr{R}^2 = 2600$ (figure 8) these two rolls completely fill the container. This process of the annihilation of a roll is similar to that associated with the transition in rolls with decreasing aspect ratio in the linear stability theory of the quiescent state (Charlson & Sani 1970). Such a continuous transition is in agreement with some recent heat-transfer studies of Koschmieder (1974), in which no distinct change in slope was observed in the Nusselt number correlation as the number of rolls decreased in a thin fluid layer. Moreover, as in Koschmieder's observations the effective wavenumber decreases as the Rayleigh number is increased but the cell is annihilated at the outer edge of the container and not at the centre as he observed at much larger aspect ratios. The decrease in the number of rolls, i.e. the decrease in the effective wavenumber, with increasing supercritical Rayleigh number is typical of all the cases investigated in this study. This wavenumber variation is in agreement with the theoretical results of Davis (1968) and experimental observations for systems with large aspect ratios (Koschmeider 1966; Rossby 1969; Krishnamurti 1970; Willis, Deardorff & Somerville

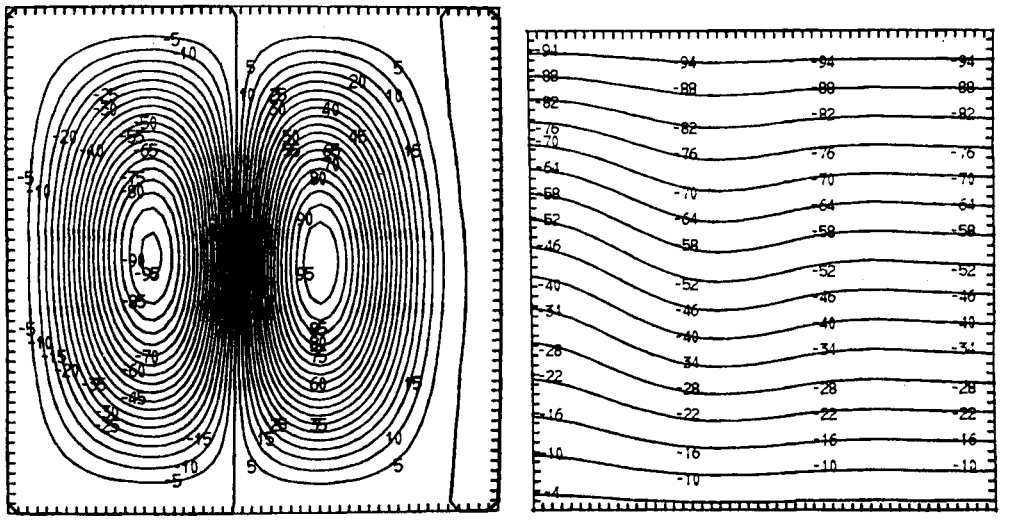

(*a*) (*b*)

FIGURE 6. (*a*) Streamlines and (*b*) isotherms for upflow solution with a conducting lateral wall; $\gamma = 2{\cdot}66$, $Pr = 1{\cdot}0$, $\mathscr{R}^2 = 1880$.

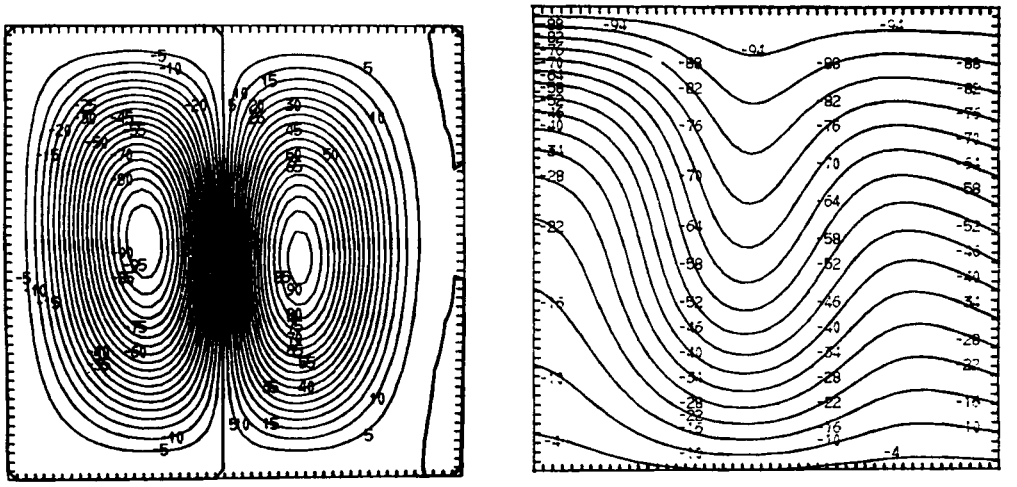

(*a*) (*b*)

FIGURE 7. (*a*) Streamlines and (*b*) isotherms for upflow solution with a conducting lateral wall; $\gamma = 2{\cdot}66$, $Pr = 1{\cdot}0$, $\mathscr{R}^2 = 2400$.

1972) but is in disagreement with the theoretical results of Schlüter, Lortz & Busse (1965) for systems of infinite lateral extent.

As a check on the calculations the streamlines and isotherms of a solution with downflow at the centre were computed for $\mathscr{R}^2 = 2600$ and $Pr = 1$. The upflow solution was calculated in the normal manner and then property (16) was used to generate initial guesses for the coefficients in the velocity and temperature expressions. The solution converged after one iteration with no change in the

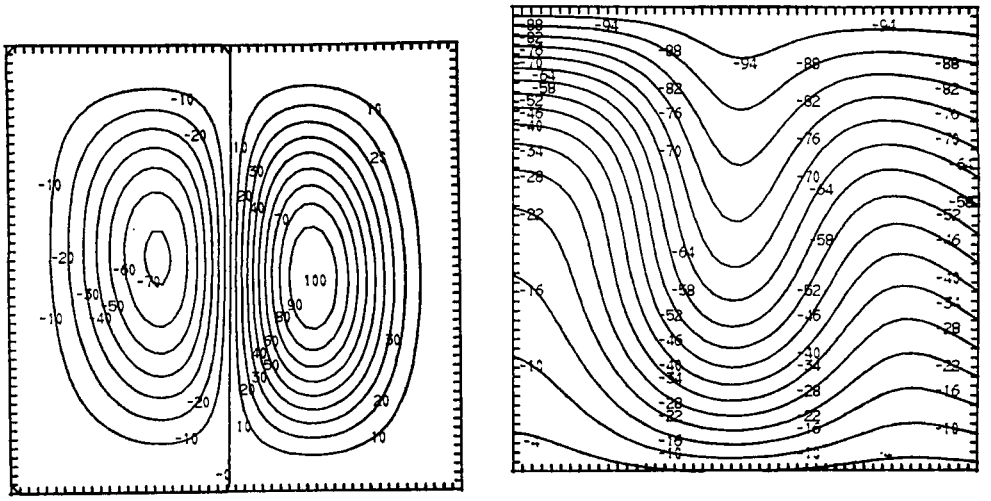

(a) (b)

FIGURE 8. (a) Streamlines and (b) isotherms for upflow solution with a conducting lateral wall; $\gamma = 2{\cdot}66$, $Pr = 1{\cdot}0$, $\mathscr{R}^2 = 2600$.

first six significant figures of the coefficients and hence provided a check on the algebraic equations and solution algorithms. The stability and vitality of the upflow and downflow solutions have identical values; however, the magnitudes of the Nusselt numbers as defined by (29) at the bottom and top are reversed. This result follows since in the case of a conducting lateral wall the only constraint on the temperature there is that the perturbations vanish. The temperature gradient is not presumed to vanish and indeed heat transfer out through the sides would be expected if the bulk of the fluid near the wall is hotter than the corresponding linear-profile value imposed at the wall. This is the case when the fluid in the outer roll is flowing up along the wall and hence hotter fluid heated by the lower surface is rising near a cooler wall. In this case, the heat flowing in through the bottom must equal the heat losses through the top and the side. The reverse is true when cooler fluid is falling near the wall. The effect results in Nusselt numbers with different magnitudes at the top and bottom. In figure 9, the Nusselt numbers at the top and bottom are presented as functions of the Rayleigh number for conducting lateral walls, $Pr = 1$, $\gamma = 2{\cdot}66$ and fluid flowing up at the centre of the layer. Since the third roll is very small, its effect on the heat transferred out through the lateral wall is small. Therefore, although cooler fluid is circulating within it near the wall, its effect on the Nusselt numbers at the top and base is only to depress the magnitudes slightly. The presence of the large second roll having upflow near the wall results in heat losses through the side and therefore the Nusselt number at the base is elevated above that at the top. Above a Rayleigh number of 2400 ($\mathscr{R}^2/\mathscr{R}^2_{\text{crit}} = 1{\cdot}33$ in figure 9), the Nusselt number at the top is a slightly convex function of the Rayleigh number. The Nusselt number at the bottom is a nearly linear function of the Rayleigh number at the larger Rayleigh numbers considered. This increasing difference between the Nusselt

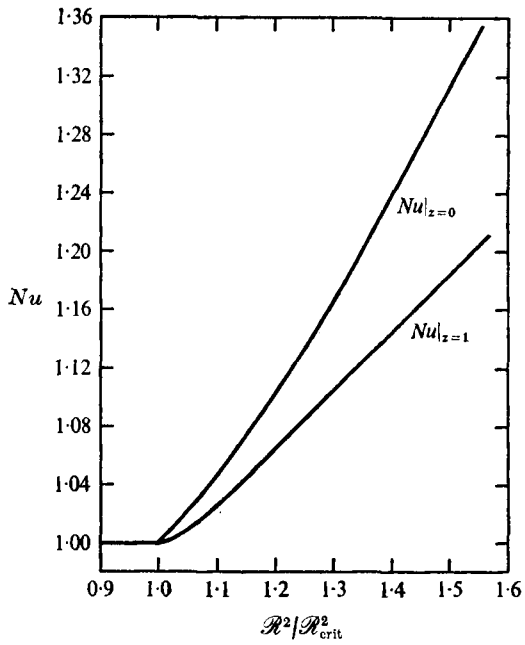

FIGURE 9. Nusselt number for upflow solution with a conducting lateral wall; $\gamma = 2{\cdot}66$, $Pr = 1{\cdot}0$.

numbers at the top and bottom suggests that a greater portion of the heat entering through the bottom surface is being rapidly conducted out through the side wall. It should be emphasized that the present treatment of the case of conducting lateral walls is mathematically convenient, but a more realistic analysis must include the solid walls and their coupling to the fluid system.

Increasing the Prandtl number from 1 to 60 at fixed $\mathscr{R}^2 = 2400$ causes a decrease in the amplitude of the convection which is reflected in a decrease in the vitality from 15·68 to 0·154. However, the appearance of 'corner rolls' has been advanced, occurring first at a Rayleigh number of 2300, although as in the case of a Prandtl number of unity, two rolls completely filling the container are not evident until $\mathscr{R}^2 > 2500$. At a Prandtl number of 0·025, the transition between three and two radials rolls occurs at only slightly supercritical Rayleigh numbers. (A similar dependence of the wavenumber on the Prandtl number has been observed by Krishnamurti (1970) in a system with large aspect ratio.) A most intriguing result at this aspect ratio is the occurrence of an oscillatory instability when the steady flow is subjected to *only* axisymmetric disturbances. At a Rayleigh number of 2088·7, the two-roll solution has transformed back to a two-roll solution with corner rolls which is now unstable to axisymmetric disturbances having a dimensionless complex exponent σ with an imaginary part of magnitude 3·21 (time for low Prandtl number analysis being in units of ν_0/L^2). This result indicates that the fluid layer has become unstable to an oscillatory flow having a fairly long period.

The flow at the transition point at which the non-oscillatory motion first becomes unstable (real part of σ zero) is a linear combination of the basic non-

oscillatory motion and an oscillatory pattern of small amplitude and long period. This behaviour is suggested by the analysis of Busse (1972) for a stress-free geometry and by the experiments of Verhoeven (1969) with mercury in thin tubes, in which oscillatory modes were observed at Rayleigh numbers 10 % above the critical value, in his case approximately $1{\cdot}2 \times 10^7$, and the experiments of Mitchell & Quinn (1966) with gases in cylindrical systems with aspect ratios near unity. However, a more detailed investigation which subjected the basic axisymmetric flow also to non-axisymmetric disturbances indicated that the flow is unstable to $n = 2$ type disturbances at a Rayleigh number of approximately 2000. Consequently, the axisymmetric oscillatory secondary flow is probably not attainable, and instead the system displays a three-dimensional flow.

Owing to computational limitations, primarily monetary, the stability analysis of the axisymmetric flow states including non-axisymmetric disturbances was limited in scope. Only a number of cases sufficient to obtain an indication of trends were investigated; moreover, only a selected number of non-axisymmetric disturbances ($n = 1, 2, 3, 4$) were included. The obvious trend in the case of unity aspect ratio, i.e. $\gamma = 1$, was that wall effects greatly enhance the stability of axisymmetric flow states. The latter persisted as stable steady states to Rayleigh numbers nearly 2·4 times critical, a value, of course, at which the quality of the approximation of the axisymmetric flow state is questionable. In contrast, for larger aspect ratios of 2·55 and 2·66 (also a few at $\gamma = 3{\cdot}00$) the general trend was that axisymmetric flow states were only stable up to 1·04–1·1 times the critical Rayleigh number. That is, axisymmetric states are not very stable. These results were initially suspect in view of Koschmieder's (1974) observations; however, all checks on the numerical algorithm as well as increases in the number of trial functions when possible indicated validity of the results. It is expected, although not established rigorously, that the approximate solutions of both the basic flow and disturbance equations should be reasonably sharp at such low supercritical Rayleigh numbers. Consequently, the present results do not confirm the dominance of the wall geometry in determining supercritical cellular structure as apparently observed by Koschmieder (1974) up to Rayleigh numbers many times the critical value. In fact, the present analysis implies the occurrence of a three-dimensional flow at slightly supercritical Rayleigh numbers. However, the stability of only a limited number of supercritical cases with an insulated lateral boundary, a better approximation to most configurations for which observations have been reported, was investigated; moreover, only the stability to axisymmetric disturbances was investigated. (See tables 6 and 7.) It appears to the authors that the disparity between the present results and experimental observations is not due primarily to the difference in aspect ratios but rather to differences in thermal conditions at the lateral wall, and currently a more detailed stability analysis of supercritical cases with an insulated lateral boundary is being carried out.† An additional general trend which was inferred from the cases examined

† A preliminary analysis of a cylindrical layer with free conducting top and bottom surfaces and a rigid conducting lateral boundary, a simpler case since the mathematical system is separable, suggests that even at large aspect ratios supercritical axisymmetric flow states are only stable to Rayleigh numbers less than 1·2–1·3 times the critical value.

was that at small values of the Prandtl number a disturbance with azimuthal wavenumber $n = 2$ is the most dangerous whereas at large values of the Prandtl number a disturbance with azimuthal wavenumber $n = 4$ is the most dangerous. In this respect it is noteworthy that Mitchell & Quinn (1966) did observe steady flows with similar azimuthal structure ($n = 2$) in cylindrical gas layers with aspect ratios near unity while operating at Rayleigh numbers approximately fifteen times the critical value.

Acknowledgement of the computer time used in this research is made to the Graduate Research Board of the University of Illinois and also to the National Center for Atmospheric Research, which is sponsored by the National Science Foundation. The authors would also like to acknowledge the valuable comments made by the reviewers.

REFERENCES

BROYDEN, C. G. 1965 *Math. Comp.* **19**, 577.

BUSSE, F. H. 1972 *J. Fluid Mech.* **52**, 97.

CHARLSON, G. S. & SANI, R. L. 1970 *Int. J. Heat Mass Transfer*, **13**, 1479.

CHARLSON, G. S. & SANI, R. L. 1971 *Int. J. Heat Mass Transfer*, **14**, 2157.

DAVIS, S. H. 1968 *J. Fluid Mech.* **32**, 619.

FINLAYSON, B. A. 1972 *The Method of Weighted Residuals and Variational Principles.* Academic.

GERSHUNI, G. Z., ZHUKOVITSKII, E. M. & TARUNIN, E. L. 1966 *Mekh. Zh. i Gaza*, **1**, 93.

GOLDSTEIN, R. J. 1964 *Chem. Engng Sci.* **19**, 997.

HOARD, C. Q., ROBERTSON, C. R. & ACRIVOS, A. 1970 *Int. J. Heat Mass Transfer*, **13**, 849.

JOSEPH, D. D. 1971 *J. Fluid Mech.* **47**, 257.

JOSEPH, D. D. & SHIR, C. C. 1966 *J. Fluid Mech.* **26**, 755.

KOSCHMIEDER, E. L. 1966 *Beitr. Phys. Atmos.* **39**, 1.

KOSCHMIEDER, E. L. 1967 *Beitr. Phys. Atmos.* **40**, 216.

KOSCHMIEDER, E. L. 1969 *J. Fluid Mech.* **35**, 527.

KOSCHMIEDER, E. L. 1974 *Adv. in Chem. Phys.* **26**, 177.

KRISHNAMURTI, R. 1970 *J. Fluid Mech.* **42**, 295.

LIANG, S. F., VIDAL, A. & ACRIVOS, A. 1969 *J. Fluid Mech.* **36**, 239.

MITCHELL, W. T. & QUINN, J. A. 1966 *A.I.Ch.E. J.* **12**, 1116.

ROSSBY, H. T. 1969 *J. Fluid Mech.* **36**, 309.

SANI, R. L. 1964 *J. Fluid Mech.* **20**, 315.

SANI, R. L. 1967 *Mathematica Japonicae*, **12**, 81.

SCHLÜTER, A., LORTZ, D. & BUSSE, F. 1965 *J. Fluid Mech.* **23**, 129.

SILVESTON, P. K. 1963 *Phys. Fluids*, **6**, 313.

SOMERSCALES, E. F. C. & DOUGHERTY, T. S. 1970 *J. Fluid Mech.* **42**, 755.

STAKGOLD, I. 1971 *SIAM Rev.* **13**, 289.

TARUNIN, E. L. 1967 *Mekh. Zh. i Gaza*, **2**, 72.

VERHOEVEN, J. D. 1969 *Phys. Fluids*, **12**, 1733.

WILLIS, G. E., DEARDORFF, J. W. & SOMERVILLE, R. C. J. 1972 *J. Fluid Mech.* **54**, 351.